A&A 448, 763–770 (2006)
DOI: 10.1051/0004-6361:20054041

Astronomy & Astrophysics

Longitudinal intensity oscillations observed with TRACE: evidence of fine-scale structure⋆

M. P. McEwan and I. De Moortel

School of Mathematics and Statistics, University of St Andrews, North Haugh, St Andrews, Fife KY169SS, Scotland
e-mail: mike@mcs.st-and.ac.uk

Received 12 August 2005 / Accepted 7 November 2005

ABSTRACT

The aim of this paper is two-fold: to increase the number of examples of observed longitudinal oscillations in coronal loops and to find evidence of the small temporal and spatial scales of these loop oscillations. Increasing the number of observed longitudinal oscillations allows for improvement in the statistics of the measured parameters, providing more accurate values for numerical and theoretical models. Furthermore, the small temporal and spatial scales of these loop oscillations could give indication of a driving force, symptomatic of coupling with the global *p*-modes. We found evidence that individual loop strands of wide coronal loop footpoints oscillate independently for short time periods. These strands have a diameter of the order of a few Mm, and the timescales on which the oscillations exist are typically less than an hour. We suggest that this is indicative of the oscillating strands being driven by the leakage of the global 5 min *p*-modes up into the corona, as simulated by De Pontieu et al. (2005, ApJ, 624, L61).
Additionally, we find 25 further examples, added to those of De Moortel et al. (2002a, Sol. Phys., 209, 89), of outwardly propagating slow MHD waves in coronal loop footpoints. The datasets are taken from JOP83, observed between April 21st 2003 and May 3rd 2003, in the TRACE 171 Å bandpass. The intensity oscillations travel outwards with a propagation speed of order $v = 99.7 \pm 3.9$ km s^{-1} and they are of small amplitude, with variations of approximately 3.7 ± 0.2% of the background intensity. These disturbances are only detected for short distances, around 8.3 ± 0.6 Mm along the loops, and the main period of oscillation is around 300 s. A second peak of period was found at around 200 s, however no correlation with the presence of a sunspot was observed within this study. Using these measured parameters we have estimated the energy flux to be of order 313 ± 26 erg cm^{-2} s^{-1}.

Key words. Sun: corona – Sun: oscillations – Sun: abundances

1. Introduction

Many questions remain unanswered about the solar corona; its fine scale structure, its heating mechanism, and the source and nature of its complicated dynamics are just a few. One method of exploring these questions is through coronal seismology (Roberts et al. 1984), using wave motions to probe into the supporting medium's secrets. Observations of coronal oscillations in the radio band were reviewed by Aschwanden (1987), reporting quasi-periodic motions of coronal loops. More recent reviews of coronal oscillations observed using the Transition Region And Coronal Explorer (TRACE) are given in e.g. Aschwanden et al. (1999), Aschwanden (2004) and Wang (2004). The technique of coronal seismology was utilised on TRACE data when Nakariakov & Ofman (2001) gave an estimate of the magnetic field strength in a coronal loop oscillating as a flare-excited, transverse kink mode. Coronal seismology relies upon the accurate measurement of wave properties in the atmosphere. The high temporal and spatial resolution of the Solar and Heliospheric Observatory (SOHO) and TRACE have provided the tools necessary to improve the number of these observations, and hence the statistics involved. A comprehensive review of analytical and numerical models combined with observations of oscillations is given in Nakariakov & Verwichte (2005).

In this paper, we will concentrate on longitudinal oscillations along coronal loops. Observations of such wave phenomena are now abundant. Nightingale et al. (1999) found propagating intensity disturbances using TRACE near coronal loop footpoints. DeForest & Gurman (1998) used SOHO to find evidence of compressive waves in plumes, which Ofman et al. (1999, 2000) interpreted as the MHD slow mode. Berghmans & Clette (1999) observed propagating intensity disturbances travelling in the corona at around 150 km s^{-1} using EIT. De Moortel et al. (2000) and Robbrecht et al. (2001) found similar outwardly propagating waves in coronal loops using TRACE data and interpreted them as coronal sound waves. Models interpreting these oscillations as damped magnetoacoustic oscillations in a stratified atmosphere were provided by Nakariakov et al. (2000) and Tsiklauri & Nakariakov (2001).

⋆ Appendices are only available in electronic form at http://www.edpsciences.org

De Moortel et al. (2002b) selected 38 such examples of outwardly propagating slow magneto-acoustic modes above the footpoints of coronal loops using TRACE 171 Å and 195 Å data. They found that oscillations along footpoints anchored in sunspot regions have a period of around 3 min and that oscillations along footpoints above regions of plage had periods of around 5 min. This suggested that both the 3 and 5 min solar oscillations may propagate up into the corona. Evidence for the propagation of the 3 min umbral oscillations throughout the solar atmosphere was previously studied in Maltby et al. (1999, 2001). A model suggesting the 5 min global *p*-modes may leak up into the corona, exciting the 5 min coronal oscillations, is given by De Pontieu et al. (2005). Joint studies have been performed using data from the TRACE instrument and SOHO/EIT by Marsh et al. (2003), observing an oscillation through chromospheric, transition region and coronal temperatures. Extensive reviews of observations and models of the slow MHD modes are in Wang (2004), De Moortel (2005) and Roberts (2005).

In this paper we aim to find evidence of the small spatial and temporal scales of the longitudinal coronal loop oscillations and to improve the statistics initially outlined in De Moortel et al. (2002a). We use TRACE data to look for longitudinal intensity oscillations above many active regions, in the lower part of coronal loops. In Sect. 2 we outline the data studied and the active regions observed. In Sect. 3 we describe our data analysis techniques and give an outline of the measured parameters. In Sect. 4 we discuss observational evidence of coupling of the global 5 min *p*-modes to the outwardly propagating slow waves and their role in the possible driving of these oscillations. Section 5 contains a statistical overview of observations from this study and the combined statistics of the previous study in De Moortel et al. (2002a). Section 6 contains the conclusions of the research and leads onto the Appendix containing the time-space diagrams and wavelet diagrams of the observed oscillating coronal loop footpoints outlined throughout this paper.

2. Data preparation and observations

The observations are taken by TRACE (Handy et al. 1999) as part of Joint Observing Programme 83 (JOP83), "High Cadence Activity Studies And The Heating Of The Corona", see Walsh et al. (1998). The data under analysis here is taken on April 21st 2003 until May 3rd 2003, and we concentrate on the 171 Å (Fe IX) passband. All of the loop footpoints observed are situated above quiescent active regions; these regions are numbered AR0339 (April 22nd 2003), AR0337 (April 24th–26th 2003), AR0346 (April 26th 2003), AR0336 (April 29th–30th 2003), AR0338 (April 29th 2003), AR0342 (April 29th 2003) and AR0345 (May 3rd 2003). The June 13th 2001 data observes AR9493.

The data has been cleaned using the TRACE preparation routines in SolarSoft Idl. In particular, dark current has been corrected for, cosmic ray hits have been removed and the images have been corrected for solar rotation. Long datasets have been trimmed so that they are uninterrupted by radiation belt transition and the South Atlantic Anomaly. They have then been sorted into sub-cubes of near constant time cadence, typically 20–30 min long with a cadence of around 50 s for some datasets to as little as 4 s cadence for others. The spatial resolution of the datasets was 1 arcsec for all datasets except those observed on April 22nd 2003, which have a spatial resolution of 0.5 arcsec.

3. Data analysis and illustration of measured parameters

The analysis of the cleaned datacubes is similar to that discussed in De Moortel et al. (2000, 2002a). We perform a running difference of the datacube which identifies propagating intensity disturbances shown as dark and light bands across the time-space diagram. We then use a wavelet analysis on the data to find the spectral and temporal information. We need to sacrifice some temporal and spatial resolution to gain information from the wavelet analysis above a certain confidence level, set at 99% for this study. We use the Morlet mother wavelet with wavelet parameter $k = 6$ as a default in this study. However, if we are dealing with a short time-series, the Paul mother wavelet is used as the effect of the cone of influence is less pronounced. A full discussion of the methods used in this analysis can be found in De Moortel et al. (2002a), and a substantial review of wavelet analysis, the wavelet parameter and the effect of varying the mother wavelet is given in De Moortel et al. (2004).

We can illustrate the measured parameters by reference to the coronal loop observed on April 30th 2003 at 1641 UT. This loop was situated above active region AR0336, close to the solar limb as shown in Fig. 1a. The time series runs from 1641 UT to 1703UT, with a near constant cadence of 14 s. The images are taken with a spatial resolution of 1″ and each frame is 512×512 pixels. The data was cleaned over two cycles using the standard Solar Soft routine trace_prep to remove cosmic ray spikes, dark current was removed and the images were corrected for solar rotation. As the time cadence is short here, we had to sum over three successive images for the running difference routine to gain a satisfactory S/N level. This routine subtracted the summed images taken approximately 84 s previously to give the time-space diagram shown in Fig. 1b.

The dark and light bands that show up in Fig. 1b, highlighted by the dashed white lines, indicate regions of decreased and increased intensity respectively, and as these bands are fairly regular we conclude that this is evidence of an oscillatory signal in intensity. The intensity (in data numbers) that corresponds to this signal, at position 4 (chosen as it shows the clearest part of the oscillation) along the loop, are shown in Fig. 1c. To find the oscillation period in the time-space diagram, we then performed a wavelet analysis on this time series. A Morlet mother wavelet was used, and the power spectrum diagram for wavelet parameter $k = 6$ at position $p = 4$ is shown in Fig. 1d. Only the regions between the time axis and the dashed lines, representing the cone of influence, showing power above the 99% confidence level are considered reliable. Wavelet parameter $k = 6$ was chosen as it gives the best temporal resolution whilst keeping the Morlet mother wavelet admissible, see Torrence & Compo (1998), and references therein for a full discussion of wavelet analysis.

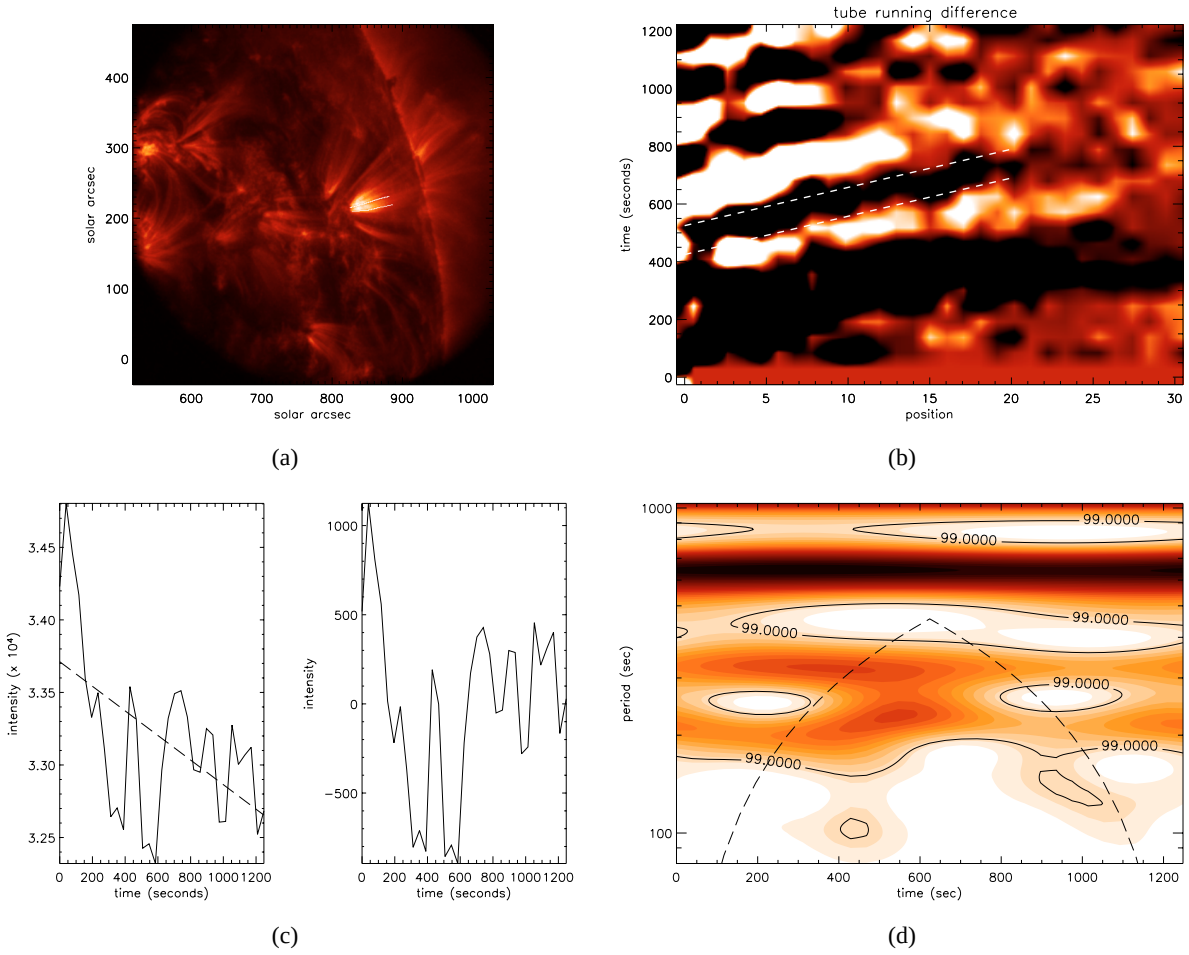

Fig. 1. a) A typical example of a large coronal loop footpoint supporting an oscillatory signal in TRACE 171 Å, from April 30th 2003, 1641 UT. The footpoint is highlighted by the solid white lines. **b)** The time-space diagram of the intensity running difference taken over the time series at each position along the loop. The dashed white lines indicate the gradient of the diagonal bands. **c)** The intensity oscillation in data numbers observed in a cut taken at position $p = 4$ along the loop, this position shows the clearest evidence of an oscillation. The left hand diagram is the data including the background intensity trend, with the right hand side being the data with an average background level removed and the linear trend (dashed line) corrected for. **d)** The wavelet diagram at position 4 along the loop. The dashed line indicates the cone of influence and the solid lines indicate the contours of 99% confidence. The darker regions indicate the areas with higher wavelet power. Only the regions between the time axis and the dashed lines, representing the cone of influence, showing power above the 99% confidence level are considered reliable.

The time series itself is 20.8 min long. The outlined loop footpoint shown in Fig. 1a is 42.0 Mm in length, and 10.4 Mm in mean width. The divergence rate of the footpoint is 0.173 along the outlined section. We estimate the propagation speed of the intensity oscillation by measuring the slope of the bands in the time-space diagram. Multiplying the inverse of this slope by the corrected spatial resolution gives an estimate of 110 $\mathrm{km\,s^{-1}}$ for this example (the corrected spatial resolution is calculated by taking the spatial resolution of the data and multiplying it by the number of pixels we have summed over for the running difference). The variation in the amplitude is given by the data in Fig. 1c, which shows a variation in amplitude from the background intensity of 1.48% to 3.89%. From a wavelet analysis we find periods ranging from 175 s to 450 s. It is clear that Fig. 1d shows two bands of period, at around 200 s and 300 s. However, taking into account all positions along the loop, we find that most power occurs with a period of around 300 s, and that this intensity oscillation is no longer detectable after travelling 11.2 Mm along the loop. In this example the loop footpoint is not anchored in a sunspot so the result of a 300 s period is consistent with De Moortel et al. (2002a).

The properties of the disturbance within the data are suggestive of a compressional wave, the speed of which is indicative of the slow MHD mode. The datasets which yield similar properties are reported in Sect. 5, as is the updated set of statistics of the various parameters found here and in De Moortel et al. (2002a). In the next section we study the properties of a subset of the oscillations reported in Sect. 5. We find thin strands of wide coronal loops oscillating independently and describe a possible reason for this behaviour.

4. Overview of results

The suggestion that the global 5 min *p*-modes can leak up into the corona and drive the observed coronal loop oscillations was postulated and numerically simulated in

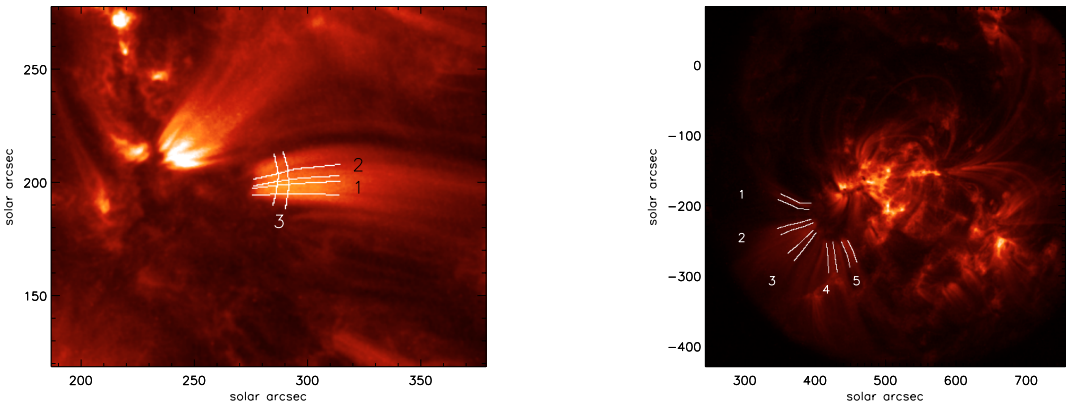

(a) (b)

Fig. 2. a) The two sections of the wide fan-like coronal loop footpoint, observed with TRACE 171 Å, that are found to oscillate independently on June 13th 2001. The strand numbered 1 oscillates at 0057 UT, whilst the strand numbered 2 oscillates at 0138 UT. **b)** The five coronal loop strands that oscillate on May 3rd 2003. The order in which these oscillate is given in Table 3.

De Pontieu et al. (2005). These authors suggested the *p*-modes leak into the chromosphere, driving the Transition Region moss oscillations. The moss oscillations have similar properties to the coronal loop oscillations. Indeed, De Pontieu et al. (2003) determined a period of 350 ± 60 s and amplitude variations of 10.0 ± 3.0%. These oscillations have a spatial extent of 1–2 arcsec, where the TRACE resolution is 1 arcsec, existing for timescales of order 30 min. They can leak up from their resonant cavity into the lower atmosphere along inclined magnetic fields, as the inclination reduces the effect of gravity. The moss oscillations become coronal shocks as they propagate up into the corona, and these shocks drive the coronal oscillations.

Previous studies have not focused directly on this temporal and spatial constraint in coronal oscillations. We show here that there is evidence of these short durations, of around 30 min, and small spatial scales occurring in wide loop footpoints in which some fine loop structure can be identified. We concentrate our analysis on data originally studied in De Moortel et al. (2002a) (June 13th 2001) as well as data taken during this study (May 3rd 2003). In both datasets we observe wide fan-like footpoints, which show some strand-like fine structure. Each strand is a few Mm in diameter, and oscillates independently and at distinct times from the others.

4.1. June 13th 2001

On June 13th 2001, TRACE observed the active region AR9493. The observation was part of JOP144, as described in De Moortel et al. (2002a). The data has a constant pointing, near constant cadence of 60 s, and 1 arcsec resolution. The co-temporal white light image contains no evidence of any sunspots. It was subject to the methods of preparation as already outlined in Sect. 2 of this paper. By taking a running difference at various times across the two outlined strands in Fig. 2a, it was found that they oscillate independently of each other at distinct times. We propose that this indicates driving of the oscillation on a small spatial scale, a few Mm in diameter, for short periods of time. This quasi-periodic driving is consistent with the behaviour of the global *p*-modes. The time-space diagrams and wavelet analysis of the data are shown in Figs. A.1a, A.1b, A.1c and A.1d presented in the Appendix.

A Morlet mother wavelet was used to analyse the time-series, with wavelet parameter $k = 6$. We found the loop strand, numbered 1 in Fig. 2a to be 13.7 Mm in length, with an average width of 3.1 Mm and a divergence rate of 0.114; the strand oscillates from 0057 UT–0126 UT, with an amplitude variation of around 6% of the background intensity. It had a period of around 350 s and a propagation speed of order 95 km s^{-1} with the oscillation being detectable for 5.7 Mm along the loop. At 0138 UT a second loop strand, numbered 2 in Fig. 2b, originating approximately 1 Mm away from the previous loop, with a length of 12.8 Mm, width of 3.4 Mm and a divergence of 0.132, was also found to oscillate. This had an amplitude of 7.1% variation of the background intensity, a period of around 390 s and a propagation speed of order 105 km s^{-1}.

The spatial scales are shown by the isolated loop strands, identified in Figs. 3a and 3b, by taking an intensity running difference across the loop. Figure 3a shows that the intensity oscillation occurs between positions 8 to 11 on the loop shown in Fig. 2a, and at a later time an oscillation occurs between positions 7 to 9. These positions correspond to strand 2 and 1 respectively in Fig. 2a. The observed oscillations are detected for around 4 to 6 cycles (or 20 to 30 min), this is indicative of the temporal constraint, as suggested by De Pontieu et al. (2005).

The results in Table 1 show that both oscillations have very similar measured parameters, with periods relatively close to the well known global 5-min oscillations. The similarity of these measurements suggests that the same driving force is the source of each oscillation. The source point itself shifts approximately 1 Mm over this time scale of 45 min, and only drives coronal oscillations in loop strands of cross-section approximately 3 Mm in diameter, fitting the postulation of *p*-mode driving of the coronal oscillations very well.

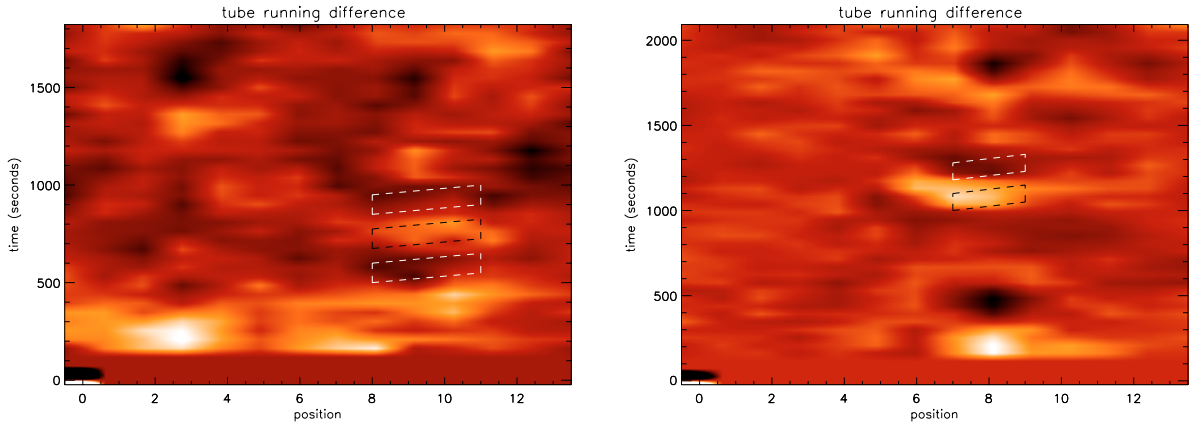

(a) (b)

Fig. 3. a) The time-space diagram of the intensity running difference taken across the loop, labelled 3 in Fig. 2a (as opposed to along) at 0057 UT on June 13th 2001. In this time-space diagram position is defined to be the position along loop 3. We see that at 0057 UT the oscillation is mainly confined around position 10 across the loop structure, corresponding to strand 2 from Fig. 2a, at this point in time. **b)** The time-space diagram along loop 3, taken on the same day at 0138 UT. We now see the intensity oscillation to be centred around position 8, this corresponds to strand 1 in Fig. 2a. Note that the original oscillation, at position 10, is no longer present.

Table 1. Overview of the measured and observed parameters from the data taken on June 13th 2001 as part of JOP144 in the 171 Å passband. L is the length of the observed footpoint, w is the average footpoint width, $w_{\rm d}$ is the divergence rate of the loop footpoint, $A_{\rm min}$–$A_{\rm max}$ is the range of intensity variation in amplitude above the background, $P_{\rm prop}$ indicates the dominant period found by wavelet analysis, v is an estimate of the propagation speed of the oscillation (where O indicates the order of the propagation speed) and $L_{\rm d}$ is the length along each footpoint that the oscillation could be detected.

No.	Time (UT)	(x, y)	L (Mm)	w (Mm)	$w_{\rm d}$	$A_{\rm min}$–$A_{\rm max}$(%)	$P_{\rm prop}$ (s)	v (km s^{-1})	$L_{\rm d}$ (Mm)
1	0057	(270,196)	13.7	3.1	0.114	2.8–9.2	350	O(95)	5.7
2	0138	(276,198)	12.8	3.4	0.132	2.8–11.4	390	O(105)	7.2

4.2. May 3rd 2003

A second set of examples of oscillations in a wide coronal loop footpoint was observed on May 3rd 2003. The data here is taken as part of JOP83, it has a near constant y-axis pointing but the x-axis pointing shifts as the Sun rotates. There is a near constant cadence of 14 s and a spatial resolution of 1 arcsec. The co-temporal white light image contains no evidence of any sunspots. The same cleaning routines were carried out as on the data taken from the June 13th 2001 datasets. Again we observe that strands oscillate independently of each other: we found five strands oscillating at distinct times, switching on and off quasi-periodically, and all showing similar measured parameters. The wide footpoint in question is shown in Fig. 2b. The full set of observed loops, time-space diagrams and wavelet diagrams highlighting these oscillations, and the others from this study, are given in Figs. A.1 to A.8 of the Appendix.

Of the twelve oscillations originating from the base of this wide coronal loop footpoint (see Table 3 for details of the times that each strand was found to oscillate), we find again that the average parameters measured are consistent with each other. The range of the period over the twelve oscillations is 175–360 s, the amplitude variation ranges from 1.1 to 6.4%, and the propagation speeds ranges from the order of 60 km s^{-1} to 145 km s^{-1}. The dimensions of the footpoints are also nearly constant across the twelve oscillations studied, with no two strands being closer than 1 Mm nor further apart than 24 Mm, except strand number 1 which is isolated. These observations strongly suggest that the driving force exists on a scale of a few Mm in diameter, matching the strands' dimensions, and that the patches jump around over a scale of the order of 10 Mm. A detailed summary of the parameters measured is given in Table 2.

From Tables 1 and 2 we see clear sets of examples of intensity oscillations in the footpoints of coronal loops, interpreted as outwardly propagating slow MHD waves, that are driven in small patches, only a few Mm in diameter, at the base of the loop. The excited strands are between 3 Mm and 10 Mm in diameter, and the patches themselves appear to be of similar size, as adjacent strands of the loops in question are not excited simultaneously. These observations strongly suggest the existence of a quasi-periodic driving force, acting on regions of small spatial scales. A possible interpretation of this is that the global 5 min p-mode oscillations are leaking up into the corona and driving oscillations in the observed coronal loop footpoints, with a similar period, as suggested by e.g. Baudin et al. (1996), Marsh et al. (2003) and De Pontieu et al. (2003, 2005). Similar suggestions that the 3 min p-mode oscillations drive sunspot oscillations have been made by Brynildsen et al. (2002), O'Shea et al. (2002) and Rendtel et al. (2003).

These observations appear to support the coupling behaviour simulated numerically by De Pontieu et al. (2005): the global p-modes, normally evanescent upon reaching the

Table 2. Overview of the measured and observed parameters from the data taken on May 3rd 2003 as part of JOP83 in the 171 Å passband. Variables as defined in Table 1.

No.	Time (UT)	(x, y)	L (Mm)	w (Mm)	w_d	A_{min}–A_{max} (%)	$P_{prop}(s)$	v (km s^{-1})	L_d (Mm)
2	1605	(369, −248)	37.4	8.8	0.136	1.1–4.2	225	O(130)	5.5
5	1605	(340, −234)	30.4	9.6	0.143	2.1–5.3	175	O(100)	4.3
5	1740	(387, −247)	34.2	8.3	0.191	1.1–4.7	220	O(85)	8.9
3	1834	(359, −237)	32.3	12.4	0.315	1.1–5.6	360	O(100)	16.2
4	1858	(389, −251)	28.6	8.2	0.229	1.4–4.1	300	O(115)	7.2
5	1858	(397, −247)	31.8	9.2	0.251	1.3–5.2	300	O(60)	6.4
2	2012	(360, −228)	40.5	10.8	0.197	1.7–6.4	310	O(80)	5.8
5	2012	(407, −251)	31.3	8.7	0.139	1.5–5.6	310	O(85)	6.0
1	2301	(388, −204)	36.8	7.7	0.118	1.6–6.0	330	O(90)	6.9
1	2321	(391, −205)	34.0	8.4	0.064	1.1–4.2	310	O(80)	7.1
5	2321	(446, −249)	24.5	9.9	0.236	1.6–4.6	300	O(60)	9.3
2	2321	(393, −235)	26.4	10.9	0.275	1.8–4.6	300	O(145)	7.1

Table 3. Table showing that certain loop strands oscillate distinctly. Namely strand 2 is oscillating at 1605 UT, not at 1740 UT but again at 2012 UT. Strand 5 oscillates at 1740 UT, not at 1834 UT but is observed to oscillate again at 1858 UT.

Time (UT)	Oscillating strand
1605	2, 5
1740	5
1834	3
1858	4, 5
2012	2, 5
2301	1
2321	1, 2, 5

corona, can leak up into the solar atmosphere along inclined magnetic field lines, driving the coronal oscillations. Indeed, the inclination of the field lines decreases the effect of gravity, hence increasing the acoustic cut-off frequency and allowing the modes to propagate into the corona. The inclination of these field lines cannot often be determined, as many observed loops are not situated on the solar limb, after some days they will be above the limb, but TRACE may no longer be observing this active region. Another problem is that often the second footpoint cannot be identified, so an accurate reconstruction of the field lines is very difficult.

5. Statistics of slow MHD waves in coronal loops

The techniques used to obtain the results summarised in Tables 4 and 5, and presented in full in Tables B.1 and B.2 of Appendix B are as described in Sect. 3. The results presented in Table 4 are the measured parameters from this study alone. Those presented in Table 5 are the combination of our findings and those of De Moortel et al. (2002a). The uncertainty range associated with the statistics is taken to be the standard error in the mean, $\sigma_M = \sigma/\sqrt{n}$, where $\sigma = \sum(x-\mu)/\sqrt{n}$ is the standard deviation, μ is the mean and n is the number of samples.

We draw particular attention to the dimensions of the footpoints, which are very similar in both studies. This indicates that the studies have been carried out on loop footpoints of a similar size, of mean length 28.1 ± 1.3 Mm, mean width of 8.6 ± 0.3 Mm, and a mean divergence of 0.24 ± 0.02. The period of oscillation, measured using wavelet analysis, is almost exactly that determined in De Moortel et al. (2002a), with a period of 284.0 ± 10.4 s; the mean propagation speed of the 63 examples is found to be 99.7 ± 3.9 km s^{-1}. Note that a more rigorous analysis of the 38 examples studied by De Moortel et al. (2002a) yielded propagation speeds of the order $v = 98.3 \pm 5.5$ km s^{-1}. The oscillation periods were also confirmed using Fast Fourier Transform (FFT), and agreed with the wavelet results to within roughly 5%. All the oscillations are of small amplitude, with an intensity variation above the background of 3.7 ± 0.2%, and they are all detected over a similar length, $L_d = 8.3 \pm 0.6$ Mm.

If we assume the coronal loops to be homogeneous and the oscillations to be linear, then we can estimate the energy flux carried by the oscillations. The energy flux $F = \rho\left((\delta v)^2/2\right)v_s$, where δv is the wave velocity amplitude and we have taken v_s as a measure of the sound speed. Following De Moortel et al. (2002a), we take $v_s \approx c_s = 150$ km s^{-1} and $\rho = 5\times10^{-16}$ g cm^{-3}; this gives an average value for the energy flux of $F = 313 \pm 26$ erg cm^{-1} s^{-1}. This is only a small percentage of the total energy required to heat coronal loops. However it was discussed in Tsiklauri & Nakariakov (2001) that this estimate is a lower limit for the total energy flux as it only takes into account the contribution from a single harmonic.

The method for determining the propagation speed gives an estimate, but generally the error bars are large (due to the method of estimating gradients), so we can provide only the order of the propagation speed. Also, we stress the fact that the propagation speeds estimated here give a lower limit for the propagation speed of the slow magnetoacoustic mode as line-of-sight effects can be significant. A loop, directed parallel to the line-of-sight, supporting a compressional wave (or some other propagating intensity oscillation) will show a zero propagation speed using the technique of running difference. It could be interpreted simply as a periodic brightening of some kind. However, one lying perpendicular to the line-of-sight, supporting the same periodic intensity oscillation, will show the full

Table 4. Overview of the averages and ranges of the physical parameters of the 25 oscillating coronal loop footpoints observed in this study from April 21st 2003 until May 3rd 2003. Note that the uncertainty in the parameters is taken to be the standard error in the mean, σ_M.

Parameter	Average	Range
Footpoint Length, L	30.7 ± 2.8 Mm	7.0−54.6 Mm
Footpoint Width, w	9.3 ± 0.1 Mm	3.5−14.9 Mm
Footpoint Divergence w_d	0.18 ± 0.02	0.05−0.48
Oscillation Period, P	287.0 ± 17.3 s	150−550 s
Propagation Speed, v	98.4 ± 6.0 km s^{-1}	$O(60)$−$O(145)$ km s^{-1}
Relative Amplitude, A	3.4% ± 0.2%	0.7−13.4%
Detection Length, L_d	8.0 ± 1.2 Mm	2.9−18.1 Mm
Energy Flux, F	268 ± 79 erg cm^{-2} s^{-1}	68−1560 erg cm^{-2} s^{-1}

Table 5. Statistical overview of the averages and ranges of the physical properties of the 63 oscillations in coronal loop footpoints found in this study combined with that in De Moortel et al. (2002a). Note that the uncertainty in the parameters is taken to be the standard error in the mean, σ_M.

Parameter	Average	Range
Footpoint Length, L	28.1 ± 1.3 Mm	7.0−54.6 Mm
Footpoint Width, w	8.6 ± 0.3 Mm	3.5−14.9 Mm
Footpoint Divergence w_d	0.24 ± 0.02	0.05−0.71
Oscillation Period, P	284.0 ± 10.4 s	145−550 s
Propagation Speed, v	99.7 ± 3.9 km s^{-1}	$O(45)$−$O(205)$ km s^{-1}
Relative Amplitude, A	3.7% ± 0.2%	0.7−14.6%
Detection Length, L_d	8.3 ± 0.6 Mm	2.9−23.2 Mm
Energy Flux, F	313 ± 26 erg cm^{-2} s^{-1}	68−1560 erg cm^{-2} s^{-1}

value of the propagation speed, and any loop lying at an angle between these extremes will show a speed which is a fraction of the full value. We have not taken into account the line-of-sight effects in this study. We can estimate the average inclination of the loops studied in this paper, using the relation quoted in Robbrecht et al. (2001), that the expected angle of inclination is $\alpha = \arccos\left(v_\mathrm{p}/c_\mathrm{s}\right)$, where v_p is the propagation speed and $c_\mathrm{s} = 150$ km s^{-1} is the sound speed at around 1.0 MK. Using this method, we obtain an average angle of inclination from the vertical of the order of $48.3 \pm 2.0°$. This value is in good agreement with the inclination found by De Pontieu et al. (2005) to be necessary for the propagation of 5 min p-modes throughout the solar atmosphere.

This study, combined with the results of De Moortel et al. (2002a), has provided a substantial set of parameters, rigorously checked over 63 examples. The averages of the measured parameters have reasonably small errors, and could be confidently used to confirm the accuracy of theoretical or numerical models, as was the goal both here and in De Moortel et al. (2002a).

6. Discussion and conclusions

We have presented an overview of the measured parameters determined using the TRACE instrument to observe longitudinal intensity oscillations in coronal loop footpoints. We examined 79 data sub-cubes, in which we found 39 loops that showed evidence of intensity oscillations. Further analysis using wavelet analysis gave 25 examples of periodic intensity oscillations above a 99% confidence level. The measured parameters from these 25 examples have been summarised in Table 4, and combined statistically with 38 other examples studied in De Moortel et al. (2002a) in Table 5.

The data shows small amplitude periodic variations in intensity, suggestive of a compressional wave, with propagation speeds of the order of the coronal sound speed. The periods of these oscillations are much less than the coronal acoustic cut-off period; we interpret the disturbances as slow propagating magnetoacoustic waves. Approximately half of the original datacubes analysed contain evidence of such oscillations, and approximately one third showed evidence of the oscillations above the 99% confidence level. Hence we conclude that these oscillations are commonplace in footpoints of large coronal loops with the measured parameters given in Sect. 5.

We have confirmed the result that coronal loops embedded in regions of plage can oscillate, usually with a period of around 5 min. However, we did not find any further examples of coronal loops that were embedded in a sunspot. Hence we were unable to further the statistics regarding coronal loops rooted in sunspot regions.

Many of the loops observed in this study show evidence of filamentary behaviour. For example in Fig. 1a we see a wide coronal loop footpoint in which many individual strands can be identified, however only one of these strands is observed to oscillate at that point in time. Indeed, most of the loops observed have shown some extent of filamentary behaviour. We have used the proximity of several of these oscillations, particularly those occurring on June 13th 2001 and May 3rd 2003, to present evidence that the 5 min coronal oscillations could be driven by the leaking of the 5 min global p-mode oscillations. De Pontieu et al. (2005) showed that the moss oscillations are driven by the leaking of the global 5 min p-modes along

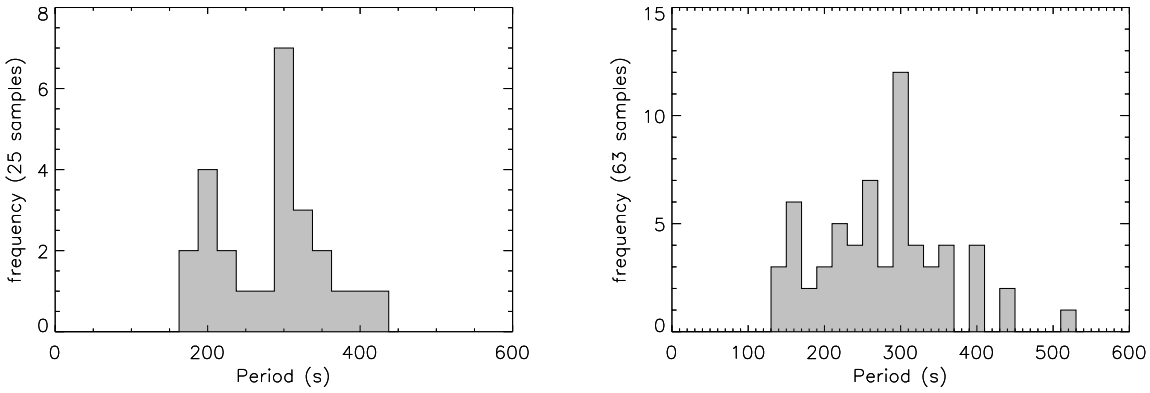

(a) (b)

Fig. 4. a) Histogram showing the distribution of the periods measured in this study. The dominant period is clearly seen at around 300 s. There is a second peak at around 200 s, as was found by De Moortel et al. (2002a). **b)** The histogram showing the distribution for all 63 examples observed. Here we see the dominant period at around 300 s with a second peak at around 160 s which is less pronounced.

inclined magnetic fields into the lower solar atmosphere, and that subsequently the moss oscillations become coronal shocks that drive the coronal loop oscillations. We showed that the coronal loop oscillations observed on June 13th 2001 and May 3rd 2003 are excited in regions of spatial extent of order 2 arcsec, which matches the temporal and spatial properties of these *p*-mode driven moss oscillations very well. This supports the idea of the quasi-periodic global *p*-modes exciting distinct strands of wide coronal loops over short timescales and is not in disagreement with the simulations performed by De Pontieu et al. (2005). This has highlighted the need for higher spatial resolution instruments in the future, as the oscillations clearly indicate a filamentary structure in coronal loops similar in size to the TRACE resolution.

Acknowledgements. M.P.M. acknowledges financial support from the Particle Physics and Astronomy Research Council and IDM acknowledges financial support from The Royal Society. The authors would also like to thank the referee for their helpful comments. The wavelet transform software was provided by C. Torrence and G. Compo and is available at URL: `http://paos.colorado.edu/research/wavelets/`.

References

Aschwanden, M. J. 1987, Sol. Phys., 111, 113
Aschwanden, M. J. 2004, Physics of The Solar Corona (Springer)
Aschwanden, M. J., Fletcher, L., Schrijver, C. J., & Alexander, D. 1999, ApJ, 520, 880
Baudin, F., Bocchialini, K., & Koutchmy, S. 1996, A&A, 314, L9
Berghmans, D., & Clette, F. 1999, Sol. Phys., 186, 207
Brynildsen, N., Maltby, P., Fredvik, T., & Kjeldseth-Moe, O. 2002, Sol. Phys., 207, 259
De Moortel, I. 2005, in MHD Waves And Oscillations In The Solar Plasma, Phil. Trans. of The Royal Society, in press
De Moortel, I., Ireland, J., & Walsh, R. W. 2000, A&A, 355, L23
De Moortel, I., Ireland, J., Walsh, R., & Hood, A. 2002a, Sol. Phys., 209, 89
De Moortel, I., Ireland, J., Hood, A., & Walsh, R. 2002b, A&A, 387, L13
De Moortel, I., Munday, S., & Hood, A. 2004, Sol. Phys., 222, 203
De Pontieu, B., Erdélyi, R., & de Wijn, A. G. 2003, ApJ, 595, L63
De Pontieu, B., Erdelyi, R., & De Moortel, I. 2005, ApJ, 624, L61
DeForest, C. E., & Gurman, J. B. 1998, ApJ, 501, L217
Handy, et al. 1999, Sol. Phys., 187, 229
Maltby, P., Brynildsen, N., Fredvik, T., Kjeldseth-Moe, O., & Wilhelm, K. 1999, Sol. Phys., 190, 437
Maltby, P., Brynildsen, N., Kjeldseth-Moe, O., & Wilhelm, K. 2001, A&A, 373, L1
Marsh, M. S., Walsh, R. W., De Moortel, I., & Ireland, J. 2003, A&A, 404, L37
Nakariakov, V. M., & Ofman, L. 2001, A&A, 372
Nakariakov, V. M., & Verwichte, E. 2005, Living Rev. Sol. Phys., `http://www.livingreviews.org/lrsp-2005-3`
Nakariakov, V. M., Verwichte, E., Berghmans, D., & Robbrecht, E. 2000, A&A, 362, 1151
Nightingale, R. W., Aschwanden, M. J., & Hurlburt, N. E. 1999, Sol. Phys., 190, 249
Ofman, L., Nakariakov, V. M., & DeForest, C. E. 1999, ApJ, 514, 441
Ofman, L., Nakariakov, V. M., & Sehgal, N. 2000, ApJ, 533, 1071
O'Shea, E., Muglach, K., & Fleck, B. 2002, A&A, 387, 642
Rendtel, J., Staude, J., & Curdt, W. 2003, A&A, 410, 315
Robbrecht, E., Verwichte, E., Berghmans, D., et al. 2001, A&A, 370, 591
Roberts, B. 2005, in MHD Waves And Oscillations In The Solar Plasma, Phil. Trans. of The Royal Society, in press
Roberts, B., Edwin, P. M., & Benz, A. 1984, ApJ, 279
Torrence, C., & Compo, G. 1998, Bull American Meteorology Society, 79
Tsiklauri, D., & Nakariakov, V. M. 2001, A&A, 379, 1106
Walsh, R. W., Ireland, J., & De Moortel, I. 1998, `http://sohowww.nascom.nasa.gov`
Wang, T. J. 2004, ESA SP-547, 417

Online Material

Appendix A:

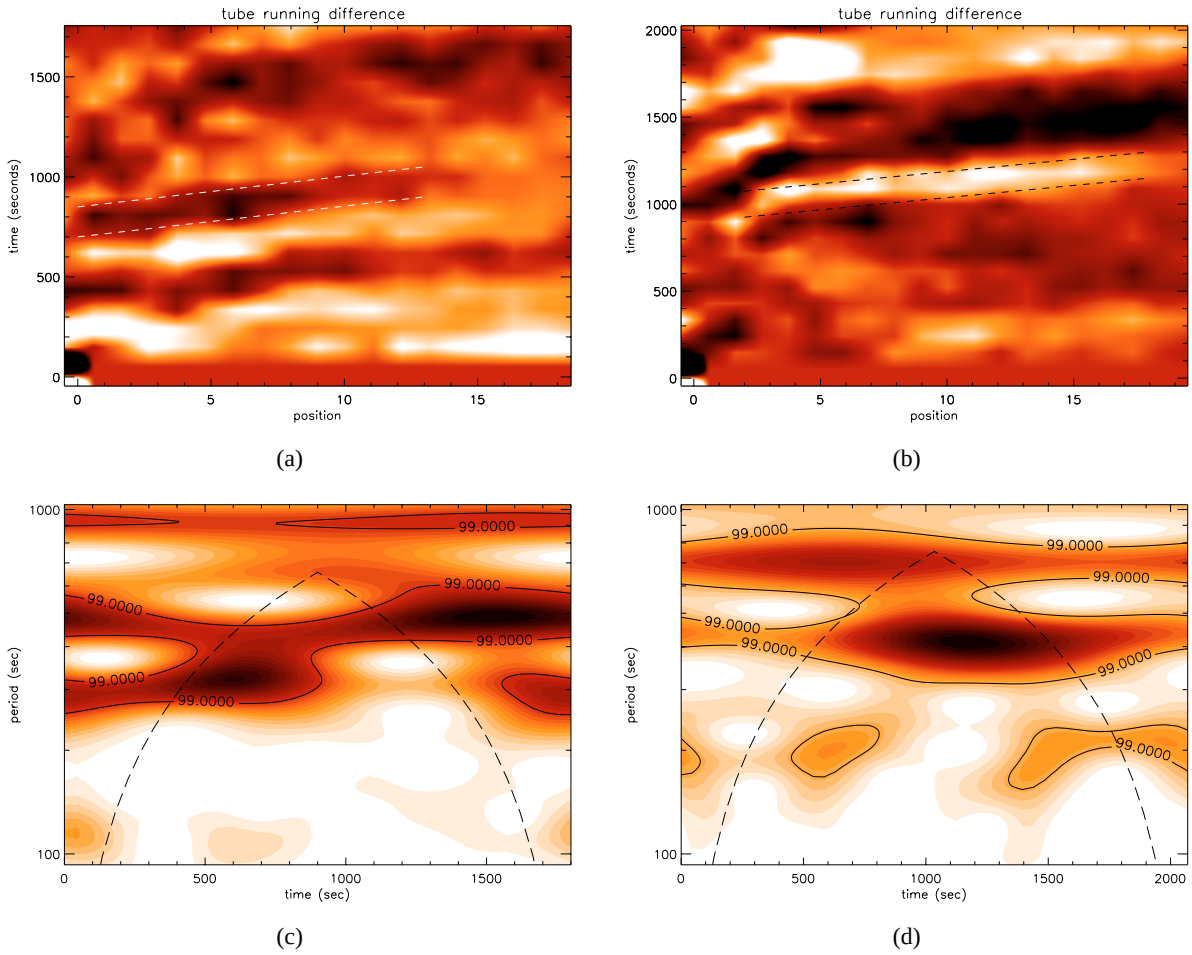

Fig. A.1. a) The time-space diagram showing intensity variation at 0057 UT on June 13th 2001 on strand 1 of the wide coronal loop footpoint. **b)** The running difference showing a similar variation in intensity at 0138 UT on the same day, on strand 2. **c)** The wavelet diagram at 0057 UT, using a Morlet mother wavelet with $k = 6$, showing a periodic variation in intensity, present throughout the time series, of around 350 s. **d)** The wavelet diagram at 0138 UT showing a period in intensity variation of around 390 s.

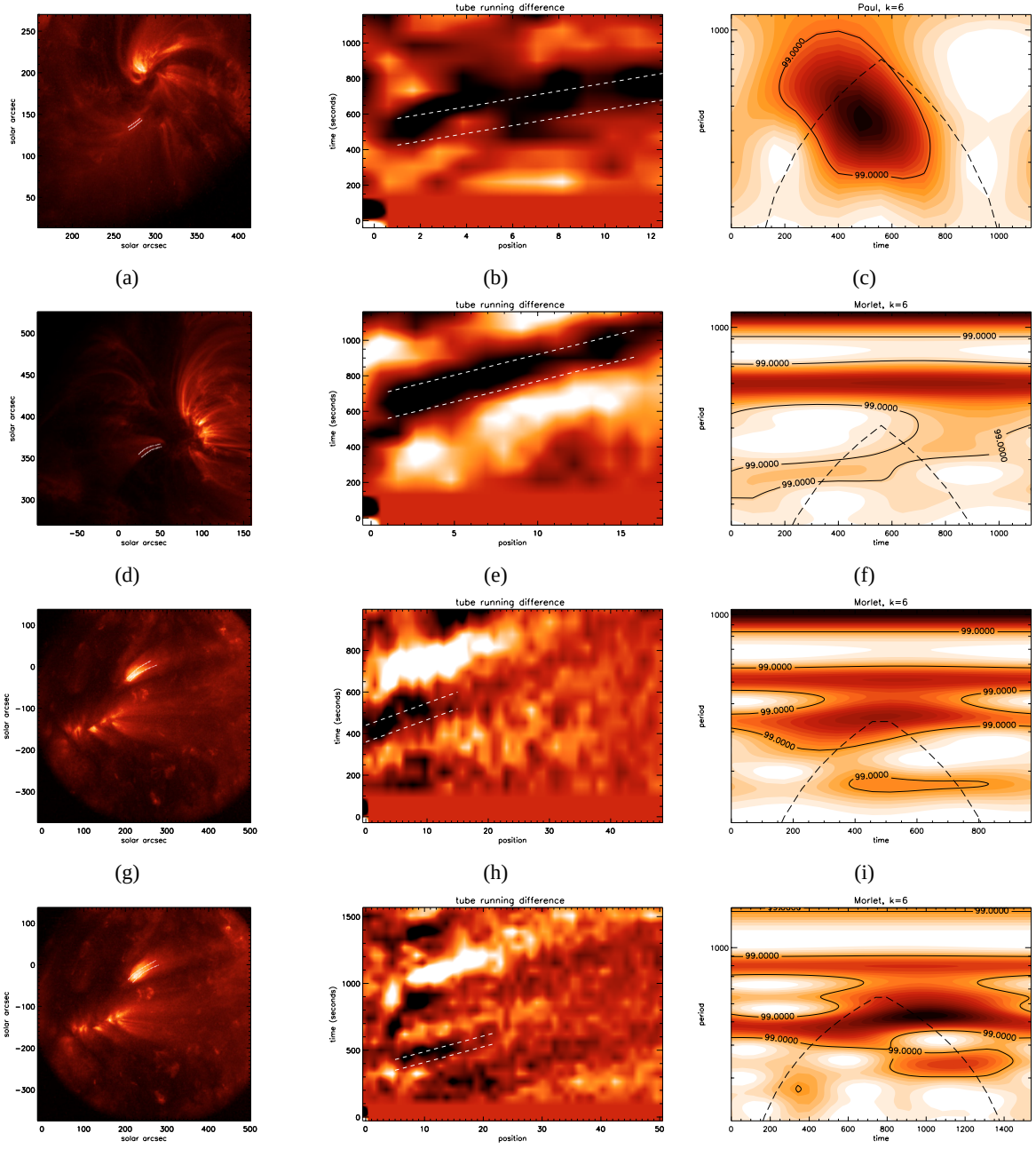

Fig. A.2. Note: all wavelet diagrams represent the signal analysed with the Morlet mother wavelet with $k = 6$, unless stated otherwise. **a)–c)** Show the coronal loop, time-space diagram and the clearest wavelet diagram, at position 3 (using the Paul wavelet with $k = 6$), for the oscillation observed in Loop 1, from Table B.1. **d)–f)** Show loop 2, with wavelet diagram at position 2. **g)–i)** Show loop 3 (wavelet diagram at position 4) and **j)–l)** show loop 4 at position 9.

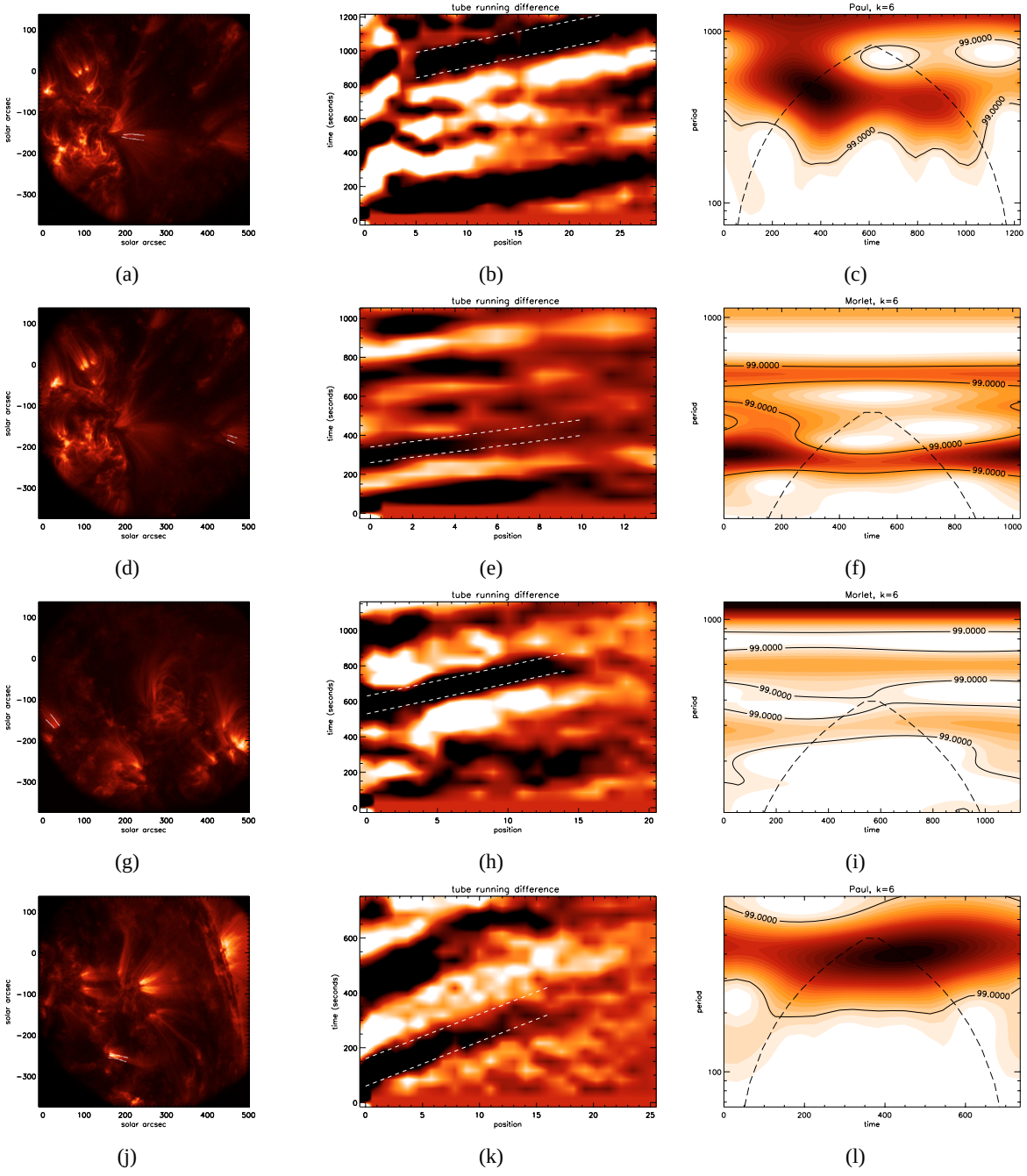

Fig. A.3. a)–c) Show the coronal loop, time-space diagram and the clearest wavelet diagram, at position 2 (using the Paul wavelet with $k = 6$), for the oscillation observed in Loop 5, from Table B.1. **d)–f)** Show loop 6, taking the wavelet diagram at position 4. **g)–i)** Show loop 7 (wavelet diagram at position 0) and **j)–l)** show loop 8 with the wavelet diagram (using the Paul wavelet with $k = 4$) at position 0.

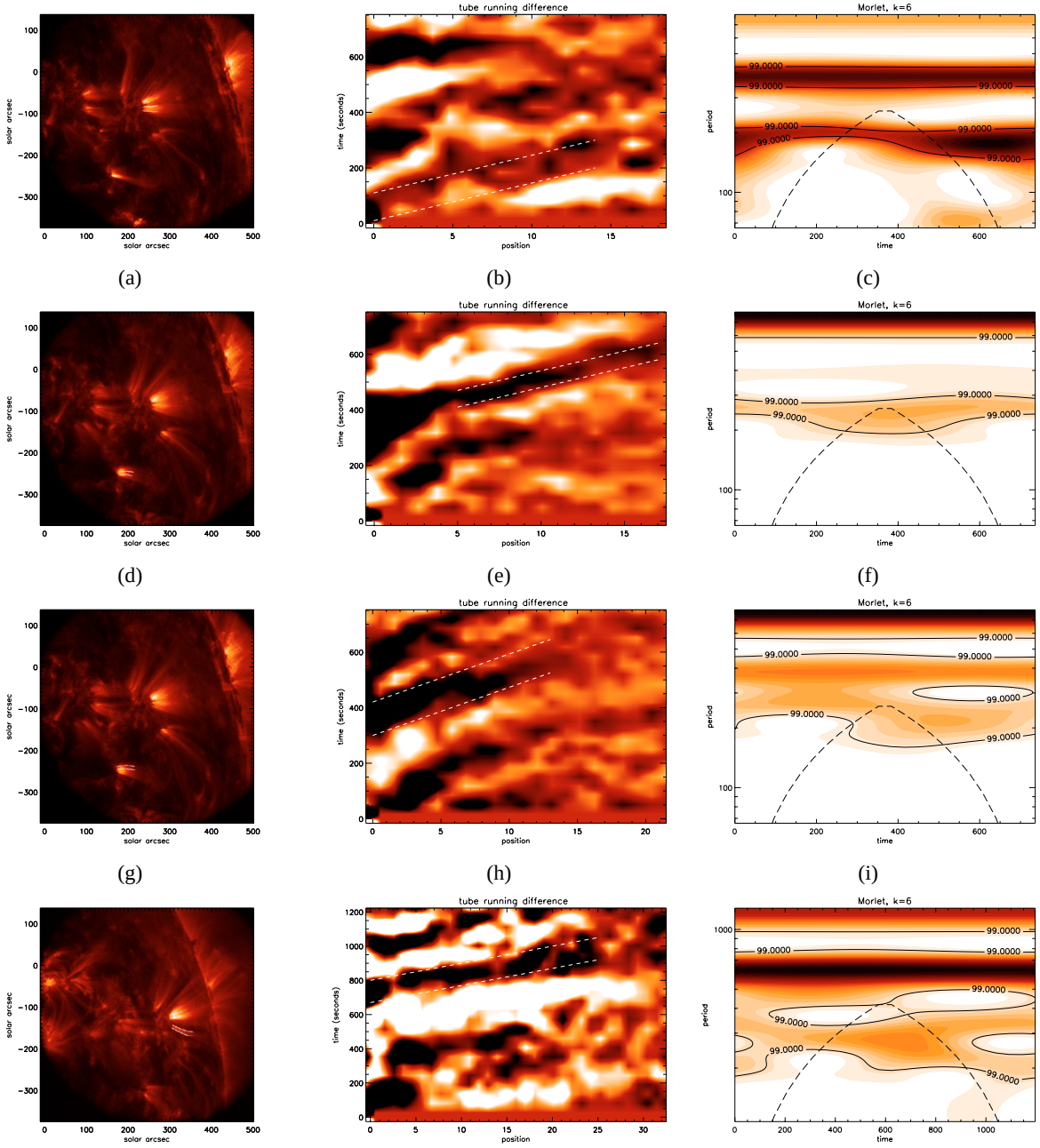

Fig. A.4. a)–c) Show the coronal loop, time-space diagram and the clearest wavelet diagram, at position 5, for the oscillation observed in Loop 9, from Table B.1. **d)–f)** Show loop 10, taking the wavelet diagram at position 4. **g)–i)** Show loop 11 (wavelet diagram at position 2) and **j)–l)** show loop 12 with the wavelet diagram at position 1.

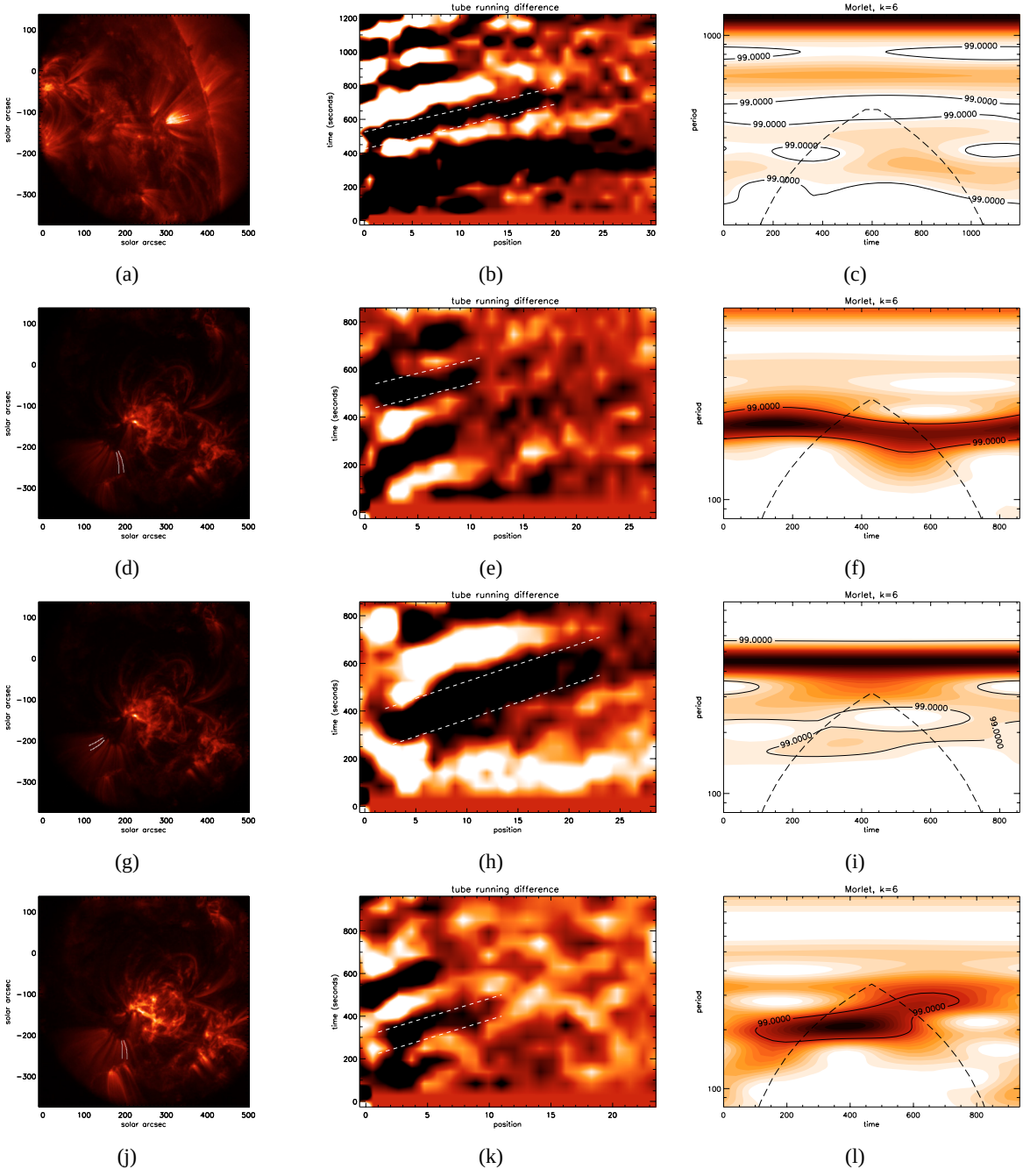

Fig. A.5. a)–c) Show the coronal loop, time-space diagram and the clearest wavelet diagram, at position 1, for the oscillation observed in Loop 13, from Table B.1. **d)–f)** Show loop 14, taking the wavelet diagram at position 6. **g)–i)** Show loop 15 (wavelet diagram at position 5) and **j)–l)** show loop 16 with the wavelet diagram at position 5.

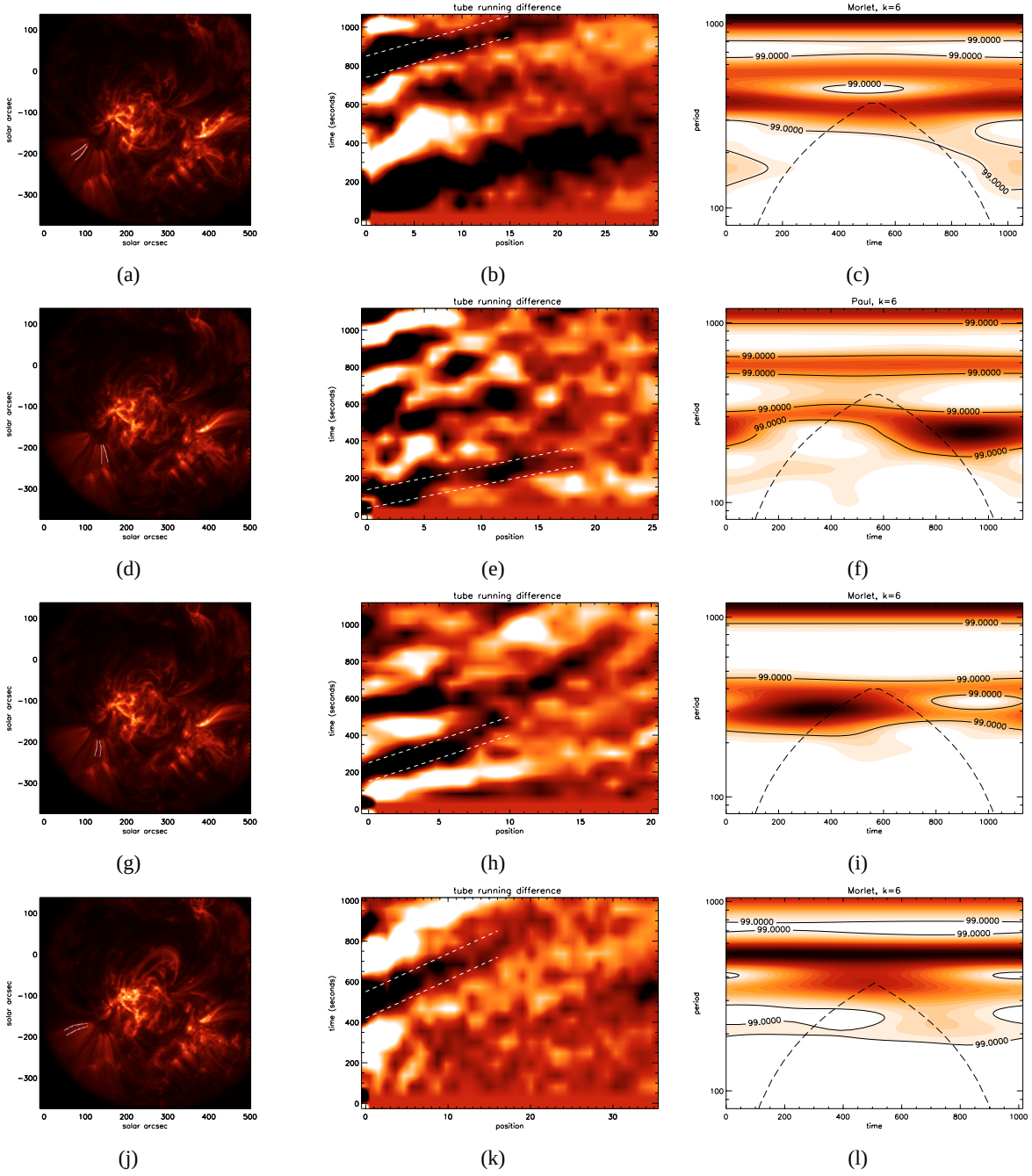

Fig. A.6. a)–c) Show the coronal loop, time-space diagram and the clearest wavelet diagram, at position 3, for the oscillation observed in Loop 17, from Table B.1. **d)–f)** Show loop 18, taking the wavelet diagram at position 1. **g)–i)** Show loop 19 (wavelet diagram at position 3) and **j)–l)** show loop 20 with the wavelet diagram at position 0.

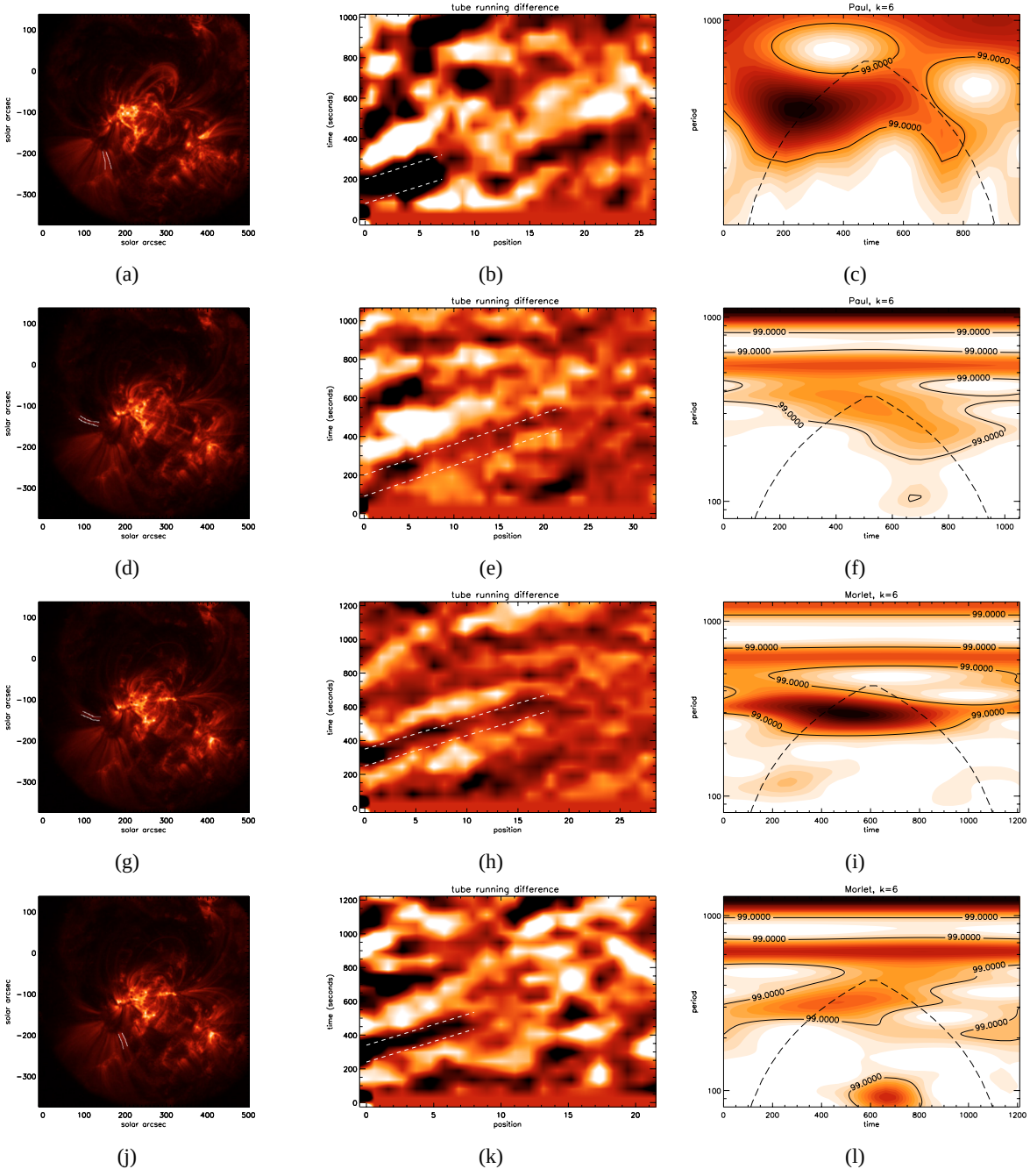

Fig. A.7. a)–c) Show the coronal loop, time-space diagram and the clearest wavelet diagram, (using the Paul wavelet with $k = 6$) at position 4, for the oscillation observed in Loop 21, from Table B.1. **d)–f)** Show loop 22, taking the wavelet diagram at position 6. **g)–i)** Show loop 23 (wavelet diagram at position 0) and **j)–l)** show loop 24 with the wavelet diagram at position 2.

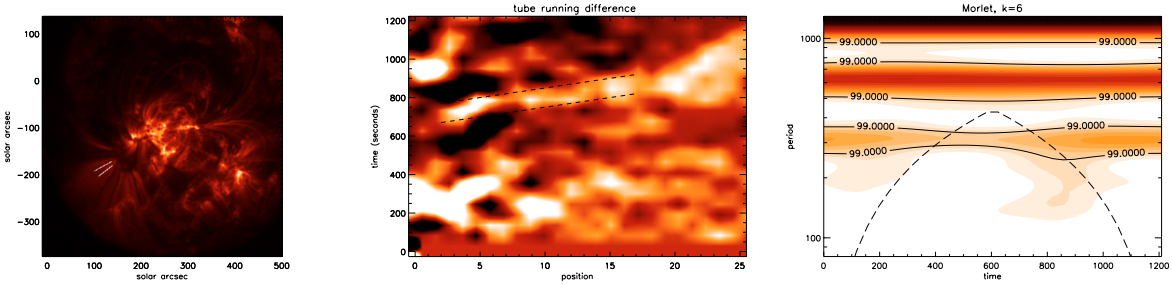

(a) (b) (c)

Fig. A.8. a)–c) Show the coronal loop, time-space diagram and the clearest wavelet diagram, at position 1, for the oscillation observed in Loop 25, from Table B.1.

Appendix B:

Table B.1. Overview of the oscillations found in JOP83 in the 171 Å bandpass of TRACE observed during the period between April 23rd 2003 and May 3rd 2003; the date and time indicate the start of the sequence (UT), AR identifies the NOAA active region number, (x, y) gives the solar x and solar y coordinates of the loop footpoint, d indicates the duration of the sequence in minutes, L is the loop length in Mm, w is the average width of the footpoint in Mm and $w_{\rm d}$ gives the divergence rate of the footpoints.

Loop	Date & Time (DDMMYY UT)	AR	(x, y)	d (min)	L (Mm)	w (Mm)	$w_{\rm d}$
1	22042003 1816	0339	(283, 142)	19.3	7.0	3.5	0.16
2	22042003 1916	0339	(51, 364)	19.3	10.0	4.7	0.29
3	24042003 0723	0337	(207, −34)	16.2	39.1	9.3	0.07
4	24042003 0849	0337	(217, −42)	25.7	54.6	12.4	0.19
5	26042003 0725	0337	(322, −152)	20.4	38.9	10.4	0.09
6	26042003 0904	0337	(377, −109)	17.4	15.6	12.0	0.23
7	26042003 1700	0346	(−522, 298)	19.8	21.0	14.9	0.48
8	29042003 1820	0336	(631, 48)	12.3	31.5	9.6	0.14
9	29042003 1820	0336	(707, 208)	12.3	25.5	10.4	0.14
10	29042003 2123	0338	(648, 51)	12.3	25.6	7.3	0.14
11	29042003 2123	0342	(646, 54)	12.3	30.1	7.7	0.05
12	30042003 1641	0336	(832, 187)	20.8	38.5	7.6	0.08
13	30042003 1641	0336	(828, 209)	20.8	42.0	10.4	0.17
14	03052003 1605	0345	(369, −248)	14.3	37.4	8.8	0.14
15	03052003 1605	0345	(340, −234)	14.3	30.4	9.6	0.14
16	03052003 1740	0345	(387, −247)	15.6	34.2	8.3	0.19
17	03052003 1834	0345	(359, −237)	17.6	32.3	12.4	0.32
18	03052003 1858	0345	(389, −251)	18.9	28.6	8.2	0.23
19	03052003 1858	0345	(397, −247)	18.9	31.8	9.2	0.25
20	03052003 2012	0345	(360, −228)	16.9	40.5	10.8	0.20
21	03052003 2012	0345	(407, −251)	16.9	31.3	8.7	0.14
22	03052003 2301	0345	(388, −204)	17.6	36.8	7.7	0.12
23	03052003 2321	0345	(391, −205)	20.0	34.0	8.4	0.06
24	03052003 2321	0345	(446, −249)	20.0	24.5	9.9	0.24
25	03052003 2321	0345	(393, −235)	20.0	26.4	10.9	0.28

Table B.2. Overview of the oscillations found in JOP83 in the 171 Å bandpass of TRACE observed during the period between April 23rd 2003 and May 3rd 2003; v is the projected speed of propagation of the wave, $A_{\rm min}-A_{\rm max}$ is the range of amplitudes relative to the background intensity, $P_{\rm min}-P_{\rm max}$ is the minimum period and maximum period found over all the positions using the wavelet analysis, $P_{\rm prop}$ is the dominant period at which the oscillations propagates, P_{fft} is the period identified using the Fast Fourier Transform, sunspot *Y* indicates a loop above a sunspot region and *N* indicates there is no sunspot observed, $L_{\rm d}$ is the length along the loop that the oscillation is detected and F is the estimated energy flux of the wave.

Loop	v	$A_{\rm min}-A_{\rm max}$	$P_{\rm min}-P_{\rm max}$	$P_{\rm prop}$	P_{fft}	Sunspot	$L_{\rm d}$	F
	km ms^{-1}	(%)	(s)	(s)	(s)	Y/N	(Mm)	(10^2 erg cm^{-2} s^{-1})
1	O(65)	2.0–5.3	250–410	340	400	N	4.2	2.8
2	O(60)	3.8–13.4	200–375	250	250	N	3.0	15.6
3	O(140)	2.0–5.9	150–330	190	180	N	3.5	3.3
4	O(120)	1.6–5.4	350–550	420	400	N	6.5	2.6
5	O(120)	2.6–6.9	275–450	440	420	N	18.1	4.8
6	O(100)	1.5–4.6	175–250	200	210	N	2.9	2.0
7	O(85)	0.8–2.8	275–400	330	315	N	9.5	0.7
8	O(90)	1.8–3.8	225–250	360	340	N	3.8	1.7
9	O(105)	0.7–3.9	200–250	215	200	N	7.1	1.1
10	O(100)	1.0–3.8	175–250	225	250	N	6.0	1.0
11	O(85)	1.3–3.5	175–250	220	225	N	5.7	1.0
12	O(145)	0.9–5.0	250–450	290	300	N	15.6	1.8
13	O(110)	1.5–3.9	175–450	300	300	N	11.2	1.5
14	O(130)	1.1–4.2	175–300	225	225	N	5.5	1.5
15	O(100)	2.1–5.3	150–310	175	175	N	4.3	2.9
16	O(85)	1.1–4.7	175–375	220	240	N	8.9	1.8
17	O(130)	1.1–5.6	275–370	360	360	N	16.2	2.4
18	O(115)	1.4–4.1	200–400	300	290	N	7.2	1.6
19	O(60)	1.3–5.2	275–325	300	280	N	6.4	2.2
20	O(80)	1.7–6.4	200–340	310	320	N	5.8	3.5
21	O(85)	1.5–5.6	225–340	310	340	N	6.0	2.7
22	O(90)	1.6–6.0	200–370	330	350	N	6.9	3.0
23	O(80)	1.1–4.2	200 –340	300	310	N	18.2	1.5
24	O(60)	1.6–4.6	200–325	300	300	N	9.3	2.0
25	O(145)	1.8–4.6	175–375	300	300	N	7.1	2.2